Simultaneously enhanced device efficiency, stabilized chromaticity of organic light emitting

diodes with lambertian emission characteristic by random convex lenses

Simultaneously enhanced device efficiency, stabilized chromaticity of organic light emitting diodes with lambertian emission characteristic by random convex lenses

Keunsoo Lee[1,2], Jonghee Lee[1], Eunhye Kim[3], Jeong-Ik Lee[1], Doo-Hee Cho[1], Jong Tae Lim[1], Chul Woong Joo[1], Joo Yeon Kim[1], Seunghyup Yoo[3], Byeong-Kwon Ju[2] and Jaehyun Moon[1]

[1] Soft I/O Interface Research Section, Electronics and Telecommunications Research Institute (ETRI), Daejeon 34129, Korea
[2] Display and Nanosystem Laboratory, College of Engineering, Korea University, Seoul 02842, Korea
[3] Department of Electrical Engineering, Korea Advanced Institute of Science and Technology (KAIST) Daejeon 34141, Korea

E-mail: jmoon@etri.re.kr and bkju@korea.ac.kr

CrossMark

Abstract

An optical functional film applicable to various lighting devices is demonstrated in this study. The phase separation of two immiscible polymers in a common solvent was used to fabricate the film. In this paper, a self-organized lens-like structure is realized in this manner with optical OLED functional film. For an OLED, there are a few optical drawbacks, including light confinement or viewing angle distortion. By applying the optical film to an OLED, the angular spectra distortion resulting from the designed organic stack which produced the highest efficiency was successfully stabilized, simultaneously enhancing the efficiency of the OLED. We prove the effect of the film on the efficiency of OLEDs through an optical simulation. With the capability to overcome the main drawbacks of OLEDs, we contend that the proposed film can be applied to various lighting devices.

S Online supplementary data available from stacks.iop.org/NANO/27/075202/mmedia

Keywords: organic light emitting diodes, light extraction, lateral polymer separation

(Some figures may appear in colour only in the online journal)

1. Introduction

Spontaneously formed structures provide a wide range of potential applications in various engineering fields. With a proper size and appropriate morphological characteristics, such structures, which apparently bear little relation to their fields of interest, can be readily applied to enhance performance levels. In this study, we examine the possibility of using a structure which is obtained via the phase separation of two immiscible polymers as an optical device. To be specific, we focus on light out-coupling in an organic light-emitting diode (OLED) using a structure which originates from polymeric phase separation. While significant advancements have been achieved in structures, organic materials and electrodes of devices [1–5], due to the presence of various light confinements, OLEDs remain associated with out-coupling of approximately 20% of the light they generate [6]. The limitation must be overcome to improve both energy savings and device lifetime. Conversely, improving the external quantum efficiency (EQE) has been found to be highly effective. The techniques used to recover wasted light are known as light-extraction techniques. Various approaches have been

suggested to extract confined light in OLEDs. Typical examples include removing the surface plasmon mode between the organic/metal cathodes [7, 8], scattering the wave-guided mode in an indium tin oxide (ITO)/organic layer [9–11], using a capping layer on the transparent top electrode [12], and refracting the glass substrate mode in a glass/air interface using a micro-lens array (MLA) [13–16].

A polymeric phase-separation structure can be obtained by dissolving immiscible components into a common solvent and then removing the solvent. During this process, immiscible components are separated spontaneously [17–19]. In general, the distribution characteristics of the separated phases are strongly influenced by the interfacial energies and bulk mixing enthalpy. The distribution can be modified by varying the processing conditions, the type of solvent used, the concentration, the molecular weight and many more variables. In this study, we choose the binary system of polystyrene (PS) and polyethylene glycol (PEG). In the thin film regime, PS and PEG separate finely in a lateral fashion with a size suitable for optical applications. The separated PEG can be removed selectively using deionized (DI) water, resulting in a film bearing a random hole array. By transferring the array using a UV-curable resin, a random convex lens (RCL) was fabricated and subsequently used for OLED external light out-coupling. We reported the effect of RCL on the blue phosphorescence OLED [20]. In the previous report, the efficiency of OLED with RCL was more improved than OLED with a commercialized MLA film, as a light extraction structure. Regarding the lightings, green light, which has a majority in white light, has to be considered. Moreover, MLA has a limitation that the enhancement is not uniform as the wavelength changes. This problem causes the unexpected color shift of OLED. Thus, it is needed to prove that the RCL can overcome this problem. We studied the integrated efficiency, luminance distribution and viewing angle characteristics by changing the thickness of the organic layer. Due to the presence of a microcavity, the efficiency of OLEDs is dependent on the device thickness. Regarding this issue, we have performed optical simulations of OLEDs as a function of organics thickness (see the supporting information). Device performance enhancement based on the microcavity approach bears two drawbacks. First, the luminance is not enhanced uniformly but selectively toward a specific direction. Second, the emission spectra show viewing angle dependency. To suppress such drawbacks, there is a need to contrive a technical mean which can yield not only uniformly enhanced luminance but also stabilized spectral characteristics. In addressing this task, we developed polymeric random convex lenses.

First, using image analyses, we quantitatively examined the size and distribution characteristics of the RCL. Second, we applied the proposed RCL to OLEDs and verified its capacity to enhance the EQE and stabilize the distortion of the angular spectrum which arises due to the weak microcavity effect [21–23], resulting from controlling organic stack. Third, in order to elucidate the light extraction of the RCL, we performed optical simulations.

2. Experiments

A lateral phase-separation structure is formed using polymer solutions which were prepared by dissolving PS ($M_w = 280\,000\,\mathrm{g\,mol^{-1}}$) and PEG ($M_w = 4000\,\mathrm{g\,mol^{-1}}$) into the common solvent of toluene. Toluene, PS and PEG were purchased from Sigma-Aldrich. To vary the fill factor, we have varied the concentration of PEG. Change in the fill factor can influence the light out-coupling. In this work, the fill factor is defined as the fractional area occupied by the PEG component. The fill factor was estimated using scanning electron microscope (SEM, Sirion FEI) images. At a PEG concentration of 27 wt.%, the fill factor reached its maximum value. In this work, we choose a PEG concentration of 7, 17 and 27 wt.%. The total concentration of polymer content was fixed as 9 wt.%. To homogenize the solutions fully, the mixtures were stirred for 24 h at room temperature. The mixtures were subsequently spin-coated at 2000 rpm for 30 s onto soda-lime glass substrates and annealed for 2 h at 120 °C in an air atmosphere to remove the solvent in the polymer film. The above process yields a polymer thin film with phase-separated PEG randomly distributed in a PS matrix. The total thickness of fabricated film was around 1 μm. The films were rinsed with DI water to remove the PEG selectively and to form PS films with randomly distributed micron-sized holes (see the supporting information). The fabricated randomly distributed hole patterns were transferred onto glass index-matching adhesive plastic film using a UV-curable resin (OrmoComp®, Micro Resist Technology). The cured resin has a refractive index of 1.52 at a wavelength of 635 nm. During the hole-pattern transfer process, a uniform pressure of 12 kPa was applied at room temperature. The fabrication scheme of the RCL is illustrated in figure 1. The fabricated RCL is expected to alter the light-traveling path on the boundary between the air and glass and to contribute to OLED light out-coupling.

The surface morphologies of the samples were measured using a SEM. The size and density of the holes on the film were analyzed quantitatively. With the commercial software image program IMAQ Vision Builder (National Instruments), we extracted the position coordinates of the holes and hole shapes. In this case, information including the coordinates, the radii of the holes and the number of holes per unit area of the phase-separated PEGs, was extracted from the SEM images of the film. We used an optical simulation with the commercial software Light Tools (Synopsys Optical Solutions Ltd) to investigate the optical effect of the film on the light out-coupling.

In order to evaluate the light-extraction capacity of the RCL, we fabricated green phosphorescence OLEDs (see the supporting information). All organic layers were deposited in a high vacuum chamber below $6.67 \times 10^{-5}\,\mathrm{Pa}$ by thermal evaporation. To protect the organics from atmospheric degradation, the fabricated OLEDs were encapsulated in glass in a glove box. The emitting area was 70 mm^2 (10 mm $\times$ 7 mm). The RCL on the glass index-matching adhesive plastic film was attached to the glass substrate of the fabricated OLED. The characteristics of a planar and MLA OLED were also
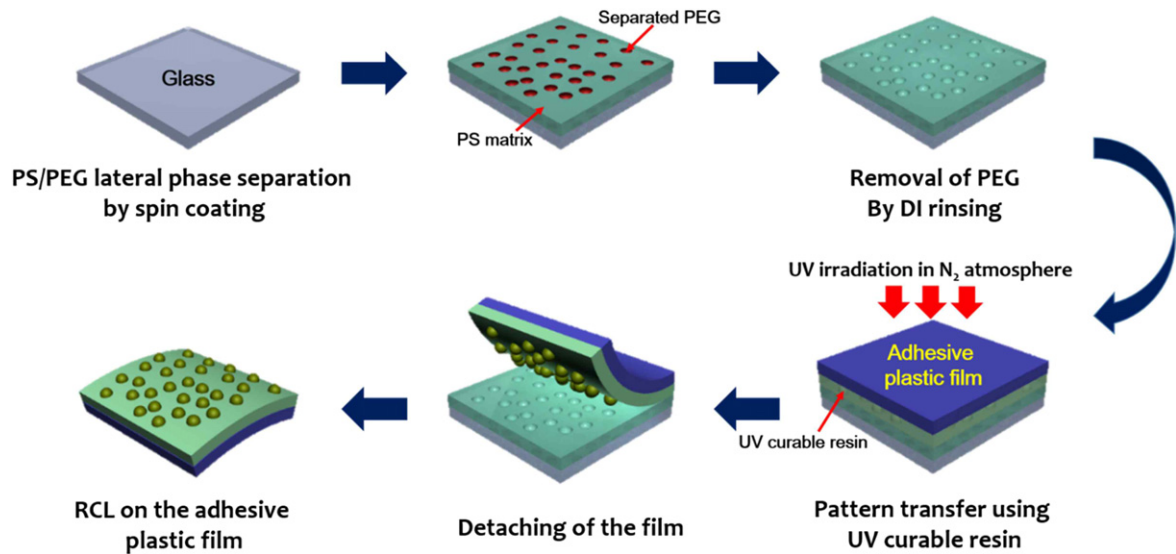
Figure 1. The fabrication process of the phase separation film and transferring the pattern to an adhesive plastic film.
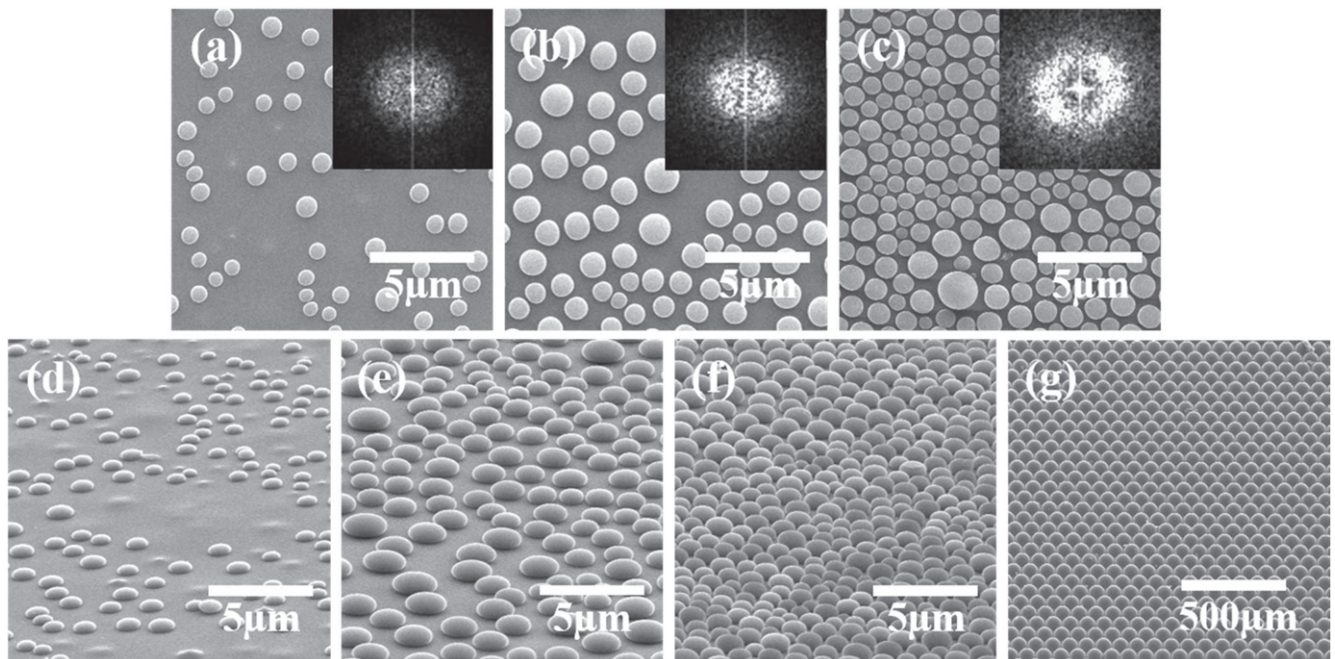

Figure 2. The SEM images of (a) RCL1, (b) RCL2, (c) RCL3 and 70° tilted images of (d) RCL1, (e) RCL2, (f) RCL3 and (g) MLA. Insets are the FT images of the corresponding SEM images.

measured for comparison with those of the RCL OLED. The angular spectra and luminance distributions were measured by a goniometer equipped a spectroradiometer (Minolta CS-2000).

3. Results and discussion

The SEM images of the surface morphologies of the RCL and MLA (Mirae Nano Tech Co.) are shown in figure 2. Figures 2(a)–(c) show top views of the RCL, with concentrations of PEG of 7 (RCL1), 17 (RCL 2) and 27 wt.% (RCL 3). The insets show Fourier transformation (FT) images

of the corresponding SEM images. All FT images are circular diffusive images with no distinct ring or spot patterns. Such features arise due to the random distributions of the RCL. Phase separation of the binary PS/PEG system takes place in a lateral fashion in the thin film regime. Phase separations of polymer blends have been investigated in various systems [24–28]. Based on time-resolved small-angle light-scattering methods, the phase separation of the PS/PMMA immiscible polymer blend was suggested to follow several sequences during a spin-coating process [25]. In the initial stage, the blend is split into two layers, in which the high-solubility component is located at the lower portion. As the film becomes thinner, instability drives the system toward a spatial

configuration of lateral phase separation, in which external factors cause the amplification of local fluctuations [29]. This PS/PMMA blend is similar to the PS/PEG system in that there are two polymers with different solubilities in a common solvent. Based on previous examinations, lateral phase separation of the PS/PEG blend is thought to have its origin in Bénard–Marangoni (BM) convection [30]. During the spin-coating process, the solvent evaporates rapidly from the surface, imposing a thermal gradient across the film thickness. The thermal gradient causes a surface-tension-driven vertical flow, which is BM convection. In our system, due to its higher solubility in toluene, PS is thought to occupy the lower portion in the initial two-layer stage. The PS-rich layer is brought up by the BM flow, where local instabilities are present, resulting in lateral phase separation. Because the system of interest is a liquid, the components can adjust their spatial configuration without mechanical constraints. The diameter size of the laterally separated PEG in our work is around 1–2 μm, which is much smaller than the previously reported PEG sizes discussed by Kim *et al* [31]. From the perspectives of BM convection, the size difference stems from the solvent evaporation rate. In contrast to the drop-casting method, not only is solvent evaporation faster but the film thickness is thinner as well. The former characteristic contributes to the mass flow and the latter induces local instability.

Figures 2(d)–(g) show tilted (70°) SEM images of the RCL and MLA. We evaluated the characteristics of the RCL distribution using the commercial software image program IMAQ Vision Builder (see the supporting information). In each RCL, the coordinates and sizes of the approximately 200 features were extracted. Figure 3(a) shows the fill factor of the RCL. The fill factors of RCL1, RCL2 and RCL3 are 14, 38 and 66%, respectively. The fill factor of the structures increases with the PEG fraction of the solution. The fill factor and initial PEG concentration show a discrepancy because the buried PS portion is excluded from the fill factor estimation. Figure 3(b) shows the distributions of the distances between each structure. The distribution tends to become narrower as the PEG concentration increases. The inter-distance frequencies of RCL1, RCL2 and RCL3 were highest at values of 13.3, 11.8 and 7.5 μm, respectively. The average distances between the structures of the RCL1, RCL2 and RCL3 samples were 14.1, 13.0 and 12.2 μm, respectively. To obtain the distributions of interparticle distances, all distinguishable features were considered. As the concentration of PEG increases, the density of the phase-separated PEG cluster also increases, decreasing the distance between the structures. Figure 3(c) shows the radii distributions of the structures. The average radii values of RCL1, RCL2 and RCL3 were 0.60, 0.80 and 0.62 μm, respectively. Under static processing conditions such as drop casting, the size of the separated domains is proportional to the viscosity of the solution [31]. A high viscosity level suppresses the coalescence of separated domains. Because the molecular weight of PS is higher than that of PEG, a high fraction of PS makes the solution viscous. The viscosities of solutions corresponding to RCL1, RCL2 and RCL3 were measured as 6.5, 6.8 and 8.8 mPa-s,

respectively. Viscosities were measured using a commercial vibro-rheometer (SV-10, A&D) at room temperature. In this situation, the size of the separated domain is expected to increase in the sequence of RCL1, RCL2 and RCL3. As shown in figure 3(c), RCL2 is larger than RCL1 but RCL3 is smaller than RCL2. The domain size distributions indicate that with a spin-coating step, which is a dynamic processing condition, the viscosity factor alone cannot explain the trend in the domain size. During the spin-coating process, the solvent rapidly evaporates from the solution, increasing the concentration. In this situation, previously formed domains may not easily coalesce to increase their sizes. Previous research on PS/PEG phase separation involving the use of the drop-casting method reported domain sizes on a scale of 10 μm. In our case, most of the domain sizes were in the range of 1 ∼ 2 μm. Our results allow us to infer that the solvent evaporation rate plays an important role in the final size of the domains. The polydispersities (σ/L) of RCL1, RCL2 and RCL3 were determined to be 0.29, 0.24 and 0.18, respectively. Here, σ and L are the standard deviation of the distance and the average distance between adjacent patterns, respectively. In binary systems, an ordered characteristic appears when the polydispersity value is lower than 0.1 [30]. Thus, we conclude that our structure is random rather than ordered. The randomness of distribution and size of structures can be beneficial in suppressing spectral distortion [8]. Also, due to the absence of wavelength dependency, randomly distributed patterns have the potential for use in preserving the chromaticity of the extracted white light. Due to the similar lens shapes and size distributions, the RCL can be applied as a light-extraction structure for various lighting devices. Owing to the random distribution, there is no preference in the light out-coupling direction. Thus, the application of the RCL can be useful for obtaining a uniform luminance distribution, which is important in lighting. Additionally, the viewing angle distortion which appears in a device with a resonant cavity, such as an LED or OLED, can be reduced. In order to examine the expected optical effect of the RCL, we applied it to OLEDs.

The difference in the refractive indices (*n*s) defines the angle of the escape cone. If the light travels from a layer with a high *n* toward a low *n*, significant portion of the light will be confined due to the total internal reflection (TIR) [32]. The out-coupling limit imposed by the TIR is detrimental to the efficiency and lifetime of the device. The confined light can be extracted by altering the light-traveling path. For this task, we applied the proposed RCL as an external light-extraction structure for OLED applications. Our OLED is a bottom-emissive type with a phosphorescent green emitter. The OLED stack structure is described in the supporting information.

Figures 4(a) and (b) show the angular luminance distributions (from −70° to 70°) of devices with electron transport layer (ETL) thicknesses of 30 nm and 60 nm. The luminance distributions were obtained at a constant current density level of 2.0 mA cm^{-2}. In order to explore the effects of the luminance distribution in relation to the RCL, we varied the ETL thickness to 30 nm and 60 nm. To determine
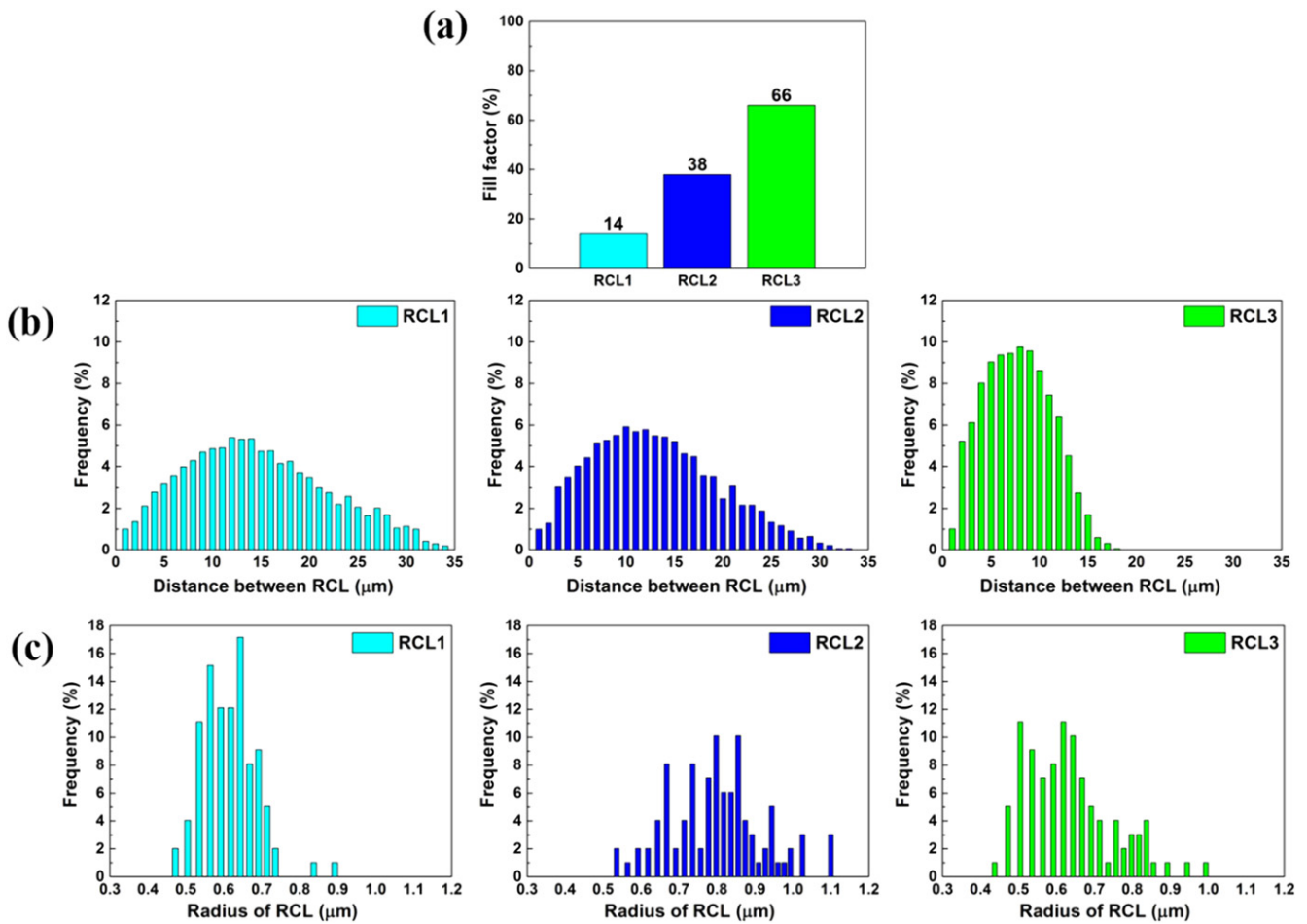
Figure 3. (a) The fill factor of RCL, (b) the frequency distribution of distance between the RCL and (c) the frequency distribution of radius of RCL.
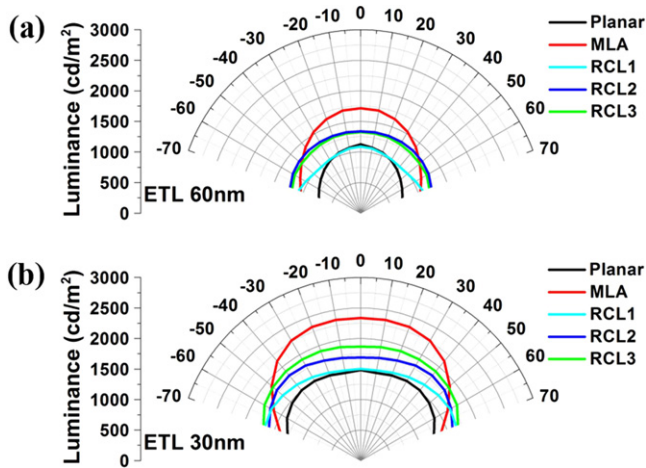

Figure 4. (a) The luminance distribution of devices (ETL 60 nm) and (b) (ETL 30 nm).

the ETL thickness, we performed optical simulations. Details of the simulations are described in the supporting information section. Commercial MLA film was used in this study for comparison with the effect of the RCL on the angular luminance distributions of OLEDs. OLEDs equipped with MLA (MLA OLED) showed selective luminance enhancements

mainly in the normal direction in both cases. In contrast, OLEDs equipped with the RCL (the RCL OLED) exhibited uniform luminance enhancements throughout the angle range. The RCL1 OLED showed no enhancement in the normal direction, whereas a gradual enhancement arose as the angle increased. As the density of the RCL increases, the selective enhancement in the normal direction also increases, resulting in a uniformly enhanced luminance distribution. As the density increases, a larger fraction of light components impinging on the substrate/air interface can alter their traveling path and can become out-coupled. In addition to the density, the aspect ratio (height/diameter) of the structures affects the luminance distribution and light out-coupling characteristics [33]. For the MLA OLEDs, enhanced luminance mainly arose in the normal direction due to the focal characteristics of the micro-lenses. Our micro-lenses are hemispherical with an aspect ratio of 1. The aspect ratio of the hemispheric shape is also 1. The luminance distributions of the OLED with the RCL exhibited light out-coupling toward high viewing angles, resulting in a uniformly enhanced luminance distribution. Our RCL has an aspect ratio of 0.6, which is lower than that of a micro-lens. Thus, it is thought that the low aspect ratio plays a role in the distribution of the light in all directions. In other words, the non-focal characteristics of the RCL contribute to
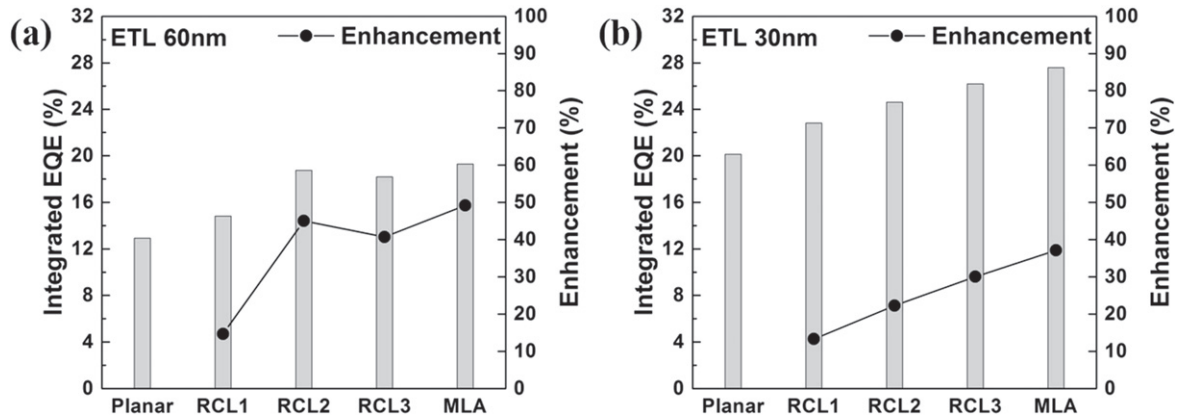
Figure 5. (a) The integrated EQE of devices (ETL 60 nm) and (b) (ETL 30 nm).

the spreading of the light out in all directions irrespective of the initial luminance distribution.

Figures 5(a) and (b) show the integrated external quantum efficiencies (EQEs, %) of the devices, as extracted using the luminance distributions in figure 4. Because the luminance distribution deviates from the Lambertian distribution, it is essential to consider the distribution when determining the efficiency values. Earlier studies only considered the normal incidence when obtaining the efficiency levels, which is only correct for a Lambertian distribution. For an ETL of 60 nm, the integrated EQE of the planar OLED was 12.9%. The integrated EQEs of RCL1, RCL2, RCL3 and of the MLA OLEDs were 14.8, 18.8, 18.2 and 19.3%, respectively, corresponding to enhancements of 14.7, 45.0, 40.7 and 49.2%. For an ETL of 30 nm, the integrated EQE of the planar OLED is 20.1%. The integrated EQEs of RCL1, RCL2, RCL3 and the MLA OLED were 22.8, 24.6, 26.2 and 27.6%, respectively, corresponding to enhancements of 13.3, 22.3, 30.1 and 37.1%. Due to the microcavity effect, the integrated EQE of the planar OLED with an ETL of 30 nm was higher than the case with an ETL of 60 nm. In accordance with the measured luminance distribution, the enhancement is proportional to the RCL density. Presumably due to the high enhancement in the normal incidence, OLEDs with MLA showed the highest integrated EQEs in both cases [20]. In the next part, we discuss this issue in terms of the EL spectra.

Figures 6(a) and (b) show the normalized angular EL spectra of the devices. For lighting devices, the angular spectrum distortion has to be minimized. The change in the spectrum not only deteriorates the original color but also changes the color perception due to the distorted emission. For the planar OLED with an ETL of 30 nm, spectrum distortion is observed due to the weak cavity effect. In the device with an ETL of 60 nm, a negligible change in the main peak position ($\lambda = 513$ nm) was observed. In addition, the full width at half maximum (FWHM) remained stable. In the ETL 30 nm case, a shift of the main peak of approximately 5 nm was observed. The FWHM also increased from 61 nm to 74 nm as the viewing angle decreased from 60° to 0°. This phenomenon was ameliorated in the ETL 60 nm case, as the effect of the weak cavity is also decreased relatively. The

OLED with the RCL shows stable angular EL spectra. As the density of the RCL increases in the OLED with an ETL of 30 nm, the variance of the FWHM does not exceed 4 nm. The change in the FWHM is virtually negligible in the OLED with an ETL of 60 nm.

Figure 7 shows the 1931 Commission internationale de l'éclairage (CIE) color coordinates. The standard deviations of the *x*- and *y*-coordinates were calculated. In the ETL 60 nm case, the standard deviations of the *x*- and *y*-coordinates were 0.006 and 0.005, 0.009 and 0.005, 0.008 and 0.005, 0.007 and 0.004, and 0.006 and 0.003, respectively, for the planar, MLA, RCL1, RCL2, and RCL3 OLED. In the ETL 30 nm case, the standard deviation of the *x*- and *y*-coordinates are 0.015 and 0.006, 0.005 and 0.002, 0.011 and 0.004, 0.004 and 0.001, and 0.004 and 0.001, respectively, for the planar, MLA, RCL1, RCL2, and RCL3 OLED. When a cavity is present (ETL 30 nm), the variance of the CIE coordinates is decreased when applying the RCL. When the weak cavity is low (ETL 60 nm), the spectrum-stabilizing effect of the RCL on the spectrum is not high. Our results indicate that the problems of EL spectra dependency affecting the viewing angle and the directed luminance distributions of the OLEDs designed with a microcavity may be ameliorated by applying our RCL. Also, design of the organic layer becomes more flexible because the viewing angle distortion resulting from the weak microcavity needed to optimize efficiency of red, green and blue of white lightings can be minimized.

In order to elucidate the light extraction capacity of the RCL, we performed an optical simulation using the commercial software Light Tools. First, an OLED device model was designed in a simulation. Then, three-dimensional images of the RCL were obtained using an atomic force microscope. The actual images were imported into the OLED simulation cells. The incident angle of the emitted light was varied from 0° to 85°. In addition, the angular distributions of the refracted light were traced to construct contour maps of the emission power.

Figure 8 shows the power contour maps of the functions of the incident and observation angles. The angular distribution of the planar OLED (figure 8(a)) shows a very narrow distribution because there is no refraction or scattering effect
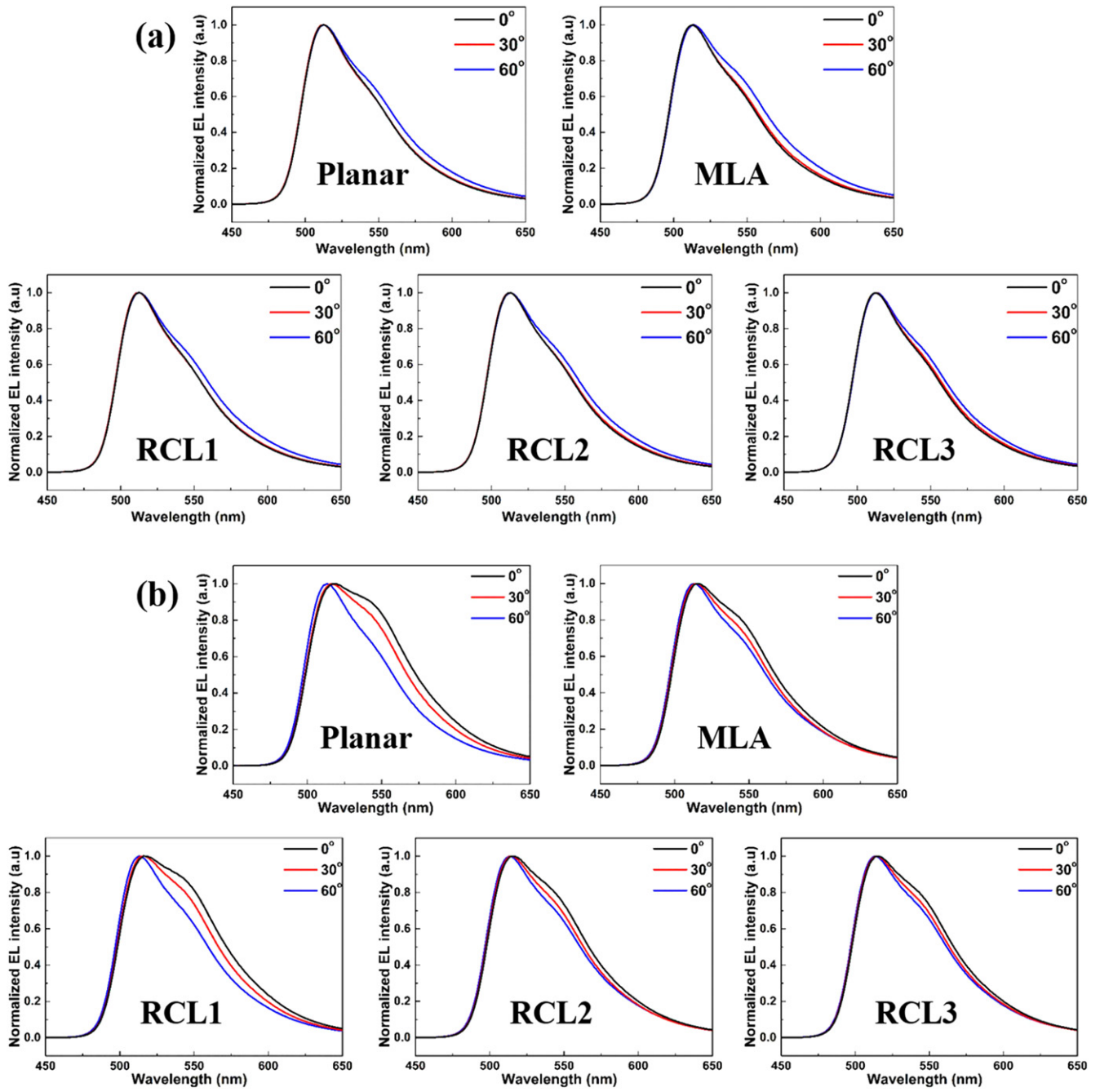
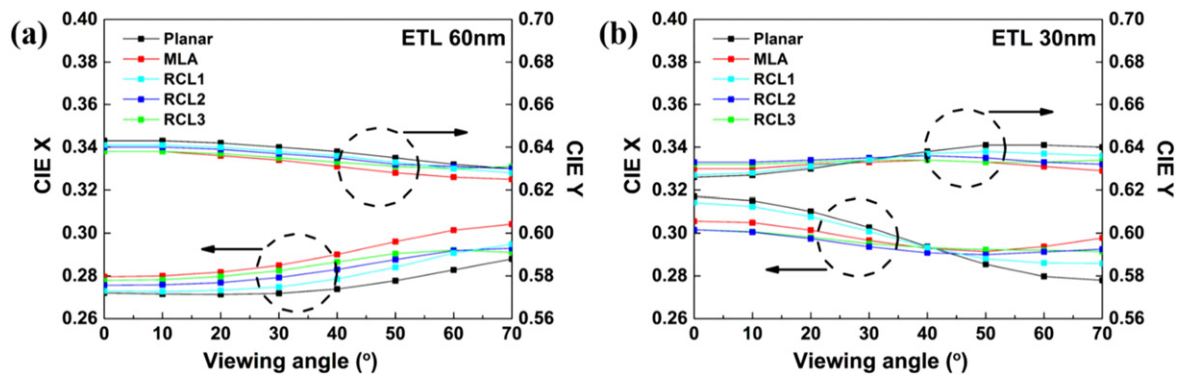**Figure 6.** (a) The angular EL spectra of devices (ETL 60 nm) and (b) (ETL 30 nm).

Figure 7. (a) The 1931 Commission internationale de l'éclairage (CIE) color coordinates of devices (ETL 60 nm) and (b) (ETL 30 nm).
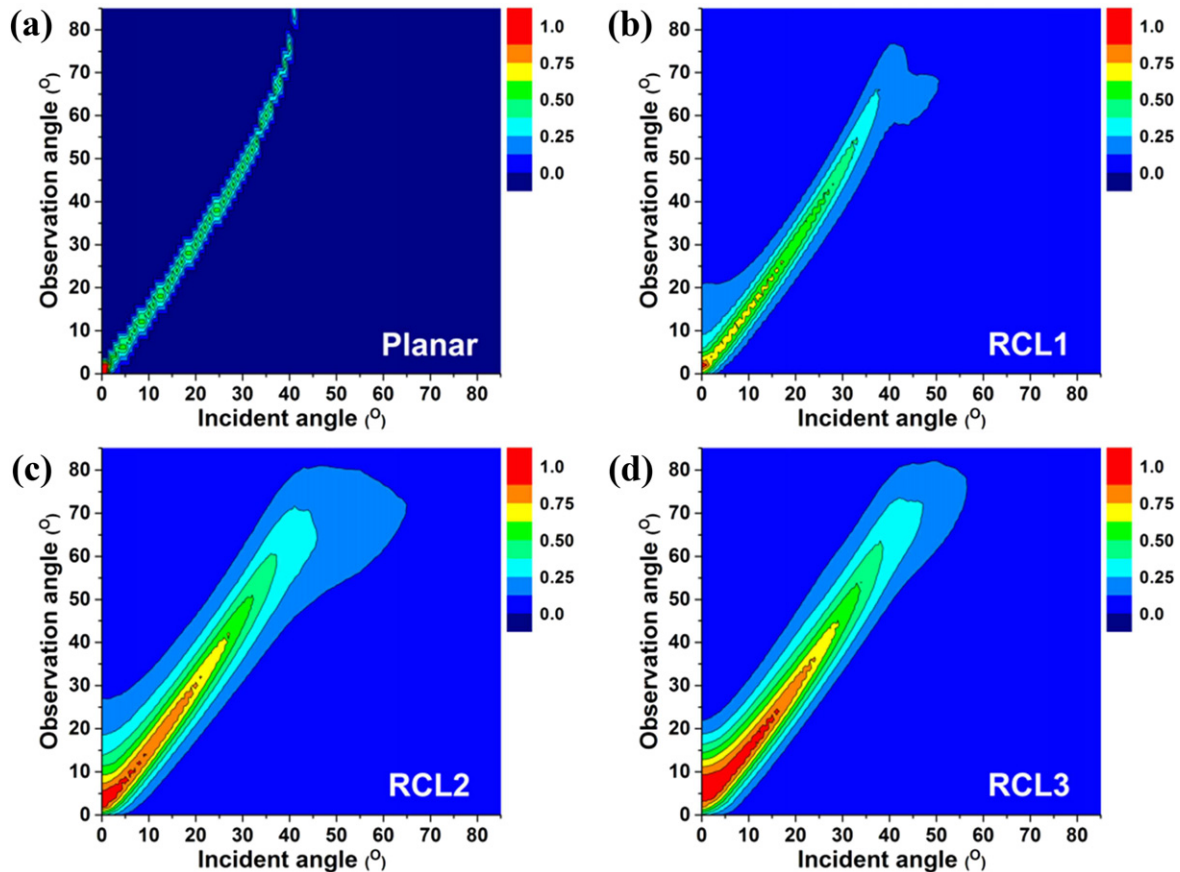
Figure 8. The angular distribution of observed light by incident angle of (a) planar, (b) RCL1, (c) RCL2 and (d) RCL3 OLED.

on the boundary between the glass substrate and the air. When the incident angle exceeds 42°, no light can be out-coupled, consistent with the value of the critical angle at the glass/air interface. Also, the range of the objection angle at set incident angle is limited. Figures 8(b)–(d) are power contour maps of the RCL OLED. As the density of the RCL increases, the angular distribution broadens and the emission power gain is enhanced. With the application of the RCL, it was possible to out-couple light up to angles of 51°, 65° and 58° corresponding to the RCL1, RCL2 and RCL3 samples, respectively. In short, the RCL OLEDs showed a larger escape angle than the planar devices. Moreover, the range of the objection angle was expanded. As the density of the RCL increases, total power of the light escaping from the glass substrate also increases because the larger RCL causes more light to be scattered or refracted. The simulation results are consistent with the experimental results. The RCL causes the incident light to scatter or refract on the boundary between the glass substrate and the air, enabling the extraction of confined light due to TIR.

4. Summary

An immiscible binary PS/PEG system undergoes lateral phase separation in the thin film regime due to the Benard–Marangoni flow. Utilizing this phase-separation feature, we fabricated films with a random convex lens and applied them onto OLEDs. OLEDs equipped with the RCL showed uniformly enhanced and distributed luminance levels throughout the angle range irrespective of the presence of a microcavity. By applying the RCL, it was possible to suppress the spectral distortion and achieve stable spectra. Optical simulations revealed that the RCL can extract the light boundary between the substrate and air. Moreover, the low aspect ratio of the RCL enables a uniform light distribution. Compared to existing commercial MLA films, our RCL film offers a better luminance distribution with stabilized spectral characteristics, making it suitable for achieving high-quality OLED lighting devices. In addition, due to the spontaneous nature of the phase separation and solution processing steps, our approach suggests a practical and viable route for fabricating large-area OLED light-extracting films.

Acknowledgments

References

[1] Sun Y, Giebink N C, Kanno H, Ma B, Thompson M E and Forrest S R 2006 *Nature* **440** 908–12

[2] Williams E L, Haavisto K, Li J and Jabbour G E 2007 *Adv. Mater.* **19** 197–202

[3] Pu Y-J, Nakata G, Satoh F, Sasabe H, Yokoyama D and Kido J 2012 *Adv. Mater.* **24** 1765–70

[4] Helander M G, Wang Z B, Qiu J, Greiner M T, Puzzo D P, Liu Z W and Lu Z H 2011 *Science* **332** 944–7

[5] Lee J, Lee J-I and Chu H Y 2009 *ETRI J.* **31** 642–6

[6] Madigan C F, Lu M-H and Sturm J C 2000 *Appl. Phys. Lett.* **76** 1650–2

[7] Kim J-B, Lee J-H, Moon C-K, Kim S-Y and Kim J-J 2013 *Adv. Mater.* **25** 3571–7

[8] Koo W H, Jeong S M, Araoka F, Ishikawa K, Nishimura S, Toyooka T and Takezoe H 2010 *Nat. Photon.* **4** 222–6

[9] Huh J W *et al* 2014 *Nanoscale* **6** 10727–33

[10] Shin J-W *et al* 2014 *Org. Electron.* **15** 196–202

[11] Kim J Y, Cho S Y and Choi K C 2013 *J. Inf. Disp.* **14** 73–7

[12] Lee J-W, Lee J, Chu H Y and Lee J-I 2013 *J. Inf. Disp.* **14** 57–60

[13] Wrzesniewski E, Eom S-H, Cao W, Hammond W T, Lee S, Douglas E P and Xue J 2012 *Small* **8** 2647–51

[14] Yang J P, Bao Q Y, Xu Z Q, Li Y Q, Tang J X and Shen S 2010 *Appl. Phys. Lett.* **97** 223303

[15] Thomschke M, Reineke S, Lüssem B and Leo K 2012 *Nano Lett.* **12** 424–8

[16] Möller S and Forrest S R 2002 *J. Appl. Phys.* **91** 3324–7

[17] Bates F S 1991 *Science* **251** 898–905

[18] Böltau M, Walheim S, Mlynek J, Krausch G and Steiner U 1998 *Nature* **391** 877–9

[19] Sung L, Karim A, Douglas J F and Han C C 1996 *Phys. Rev. Lett.* **76** 4368–71

[20] Lee K, Lee J, Joo C W, Kim J Y, Cho D-H, Lee J-I, Chu H Y, Moon J and Ju B-K 2014 *ECS Solid State Lett.* **3** R56–9

[21] Bulović V, Khalfin B, Gu G and Burrows P E 1998 *Phys. Rev. B* **58** 3730–40

[22] Epstein A, Tessler N and Einziger P D 2010 *IEEE J.Quantum Electron.* **46** 1388–95

[23] Cho S-H *et al* 2008 *Opt. Express* **16** 12632–9

[24] Walheim S, Böltau M, Mlynek J, Krausch G and Steiner U 1997 *Macromolecules* **30** 4995–5003

[25] Heriot S Y and Jones R A L 2005 *Nat. Mater.* **4** 782–6

[26] Png R-Q *et al* 2009 *Nat. Mater.* **9** 152–8

[27] Fang L, Wei M, Barry C and Mead J 2010 *Macromolecules* **43** 9747–53

[28] Spatz J P, Möller M, Noeske M, Behm R J and Pietralla M 1997 *Macromolecules* **30** 3874–80

[29] Furukawa H 1985 *Phys. Rev.* A **31** 1103–8

[30] Mitov Z and Kumacheva E 1998 *Phys. Rev. Lett.* **81** 3427–30

[31] Kim J-K, Taki K and Ohshima M 2007 *Langmuir* **23** 12397–405

[32] Hong K and Lee J-L 2011 *Electron. Mater. Lett.* **7** 77–91

[33] Kwon H, Yee Y, Jeong C-H, Na H-J and Bu J-U 2008 *J. Micromech. Microeng.* **18** 065003